

Figure 1. Schematic diagram showing the basic fluxes of water in the global hydrologic cycle. Units are cm yr^{-1} spread over the area of the land or ocean. Since the areas of land and ocean are different, the land-ocean water exchange by atmospheric transport and river runoff have different values depending on the reference area, as indicated by the parentheses. The smaller values are those referenced to the larger oceanic area. [Adapted from Hartmann, 1994]

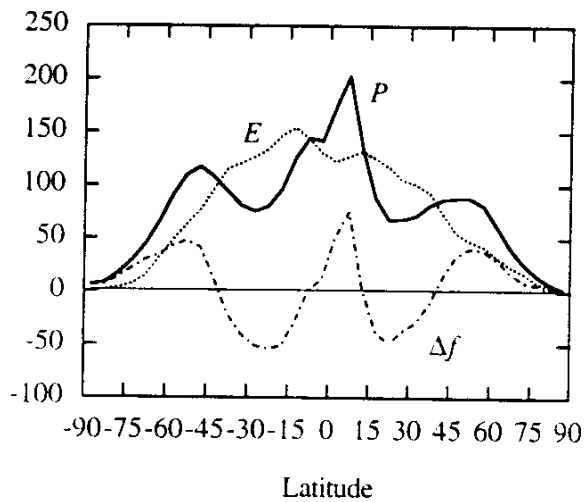


Figure 2. Latitudinal distribution of the surface hydrologic balance, showing evaporation E , precipitation P , and runoff f . [Data from Baumgartner and Reichel (1975), Reprinted from Hartmann (1994)]

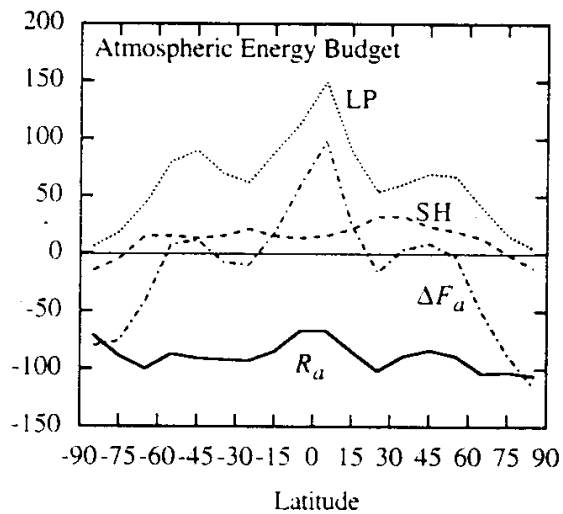


Figure 3. Distribution with latitude of the components of the atmospheric energy balance averaged over longitude and over the annual cycle. Units are W m^{-2} . [Data from Sellers (1965), Reprinted from Hartmann (1994)]

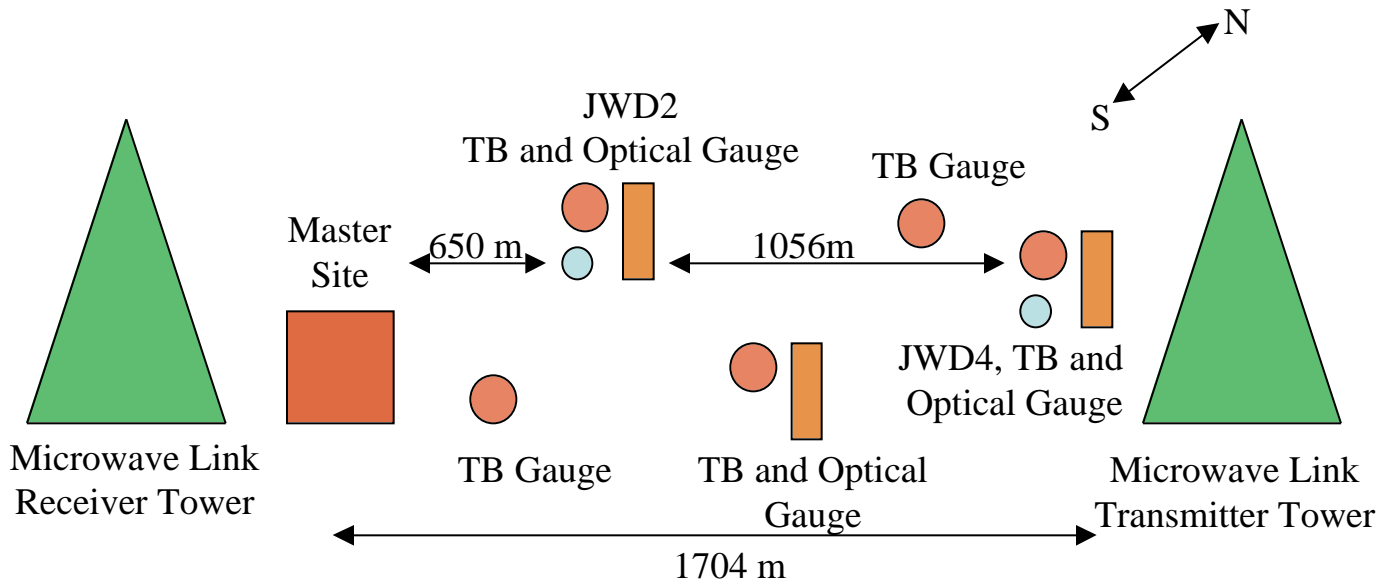


Figure 4. A schematic diagram of the Wallops Island Data Acquisition Network.

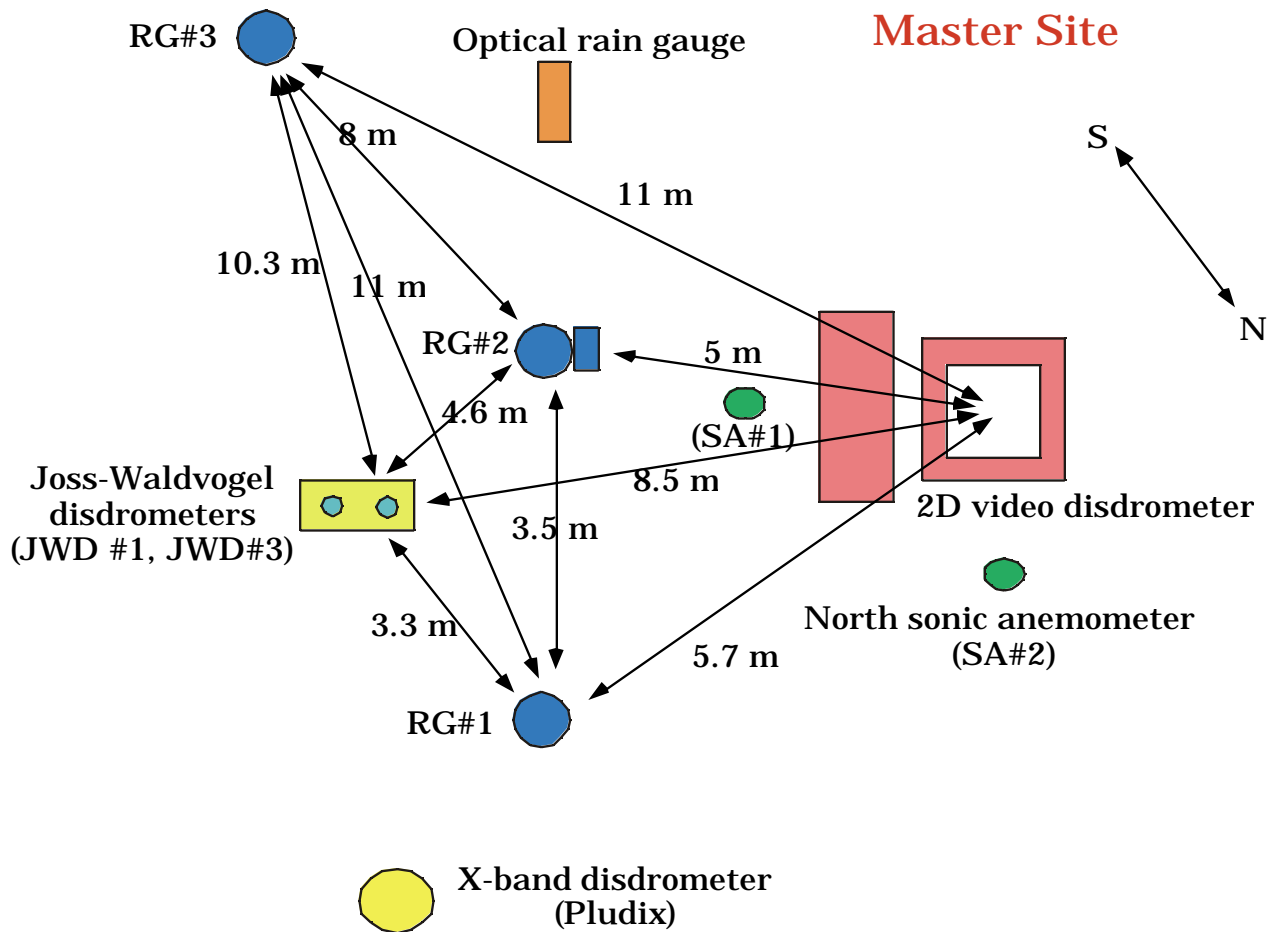


Figure 5. A schematic diagram of the master site of the Wallops Island Data Acquisition Network.

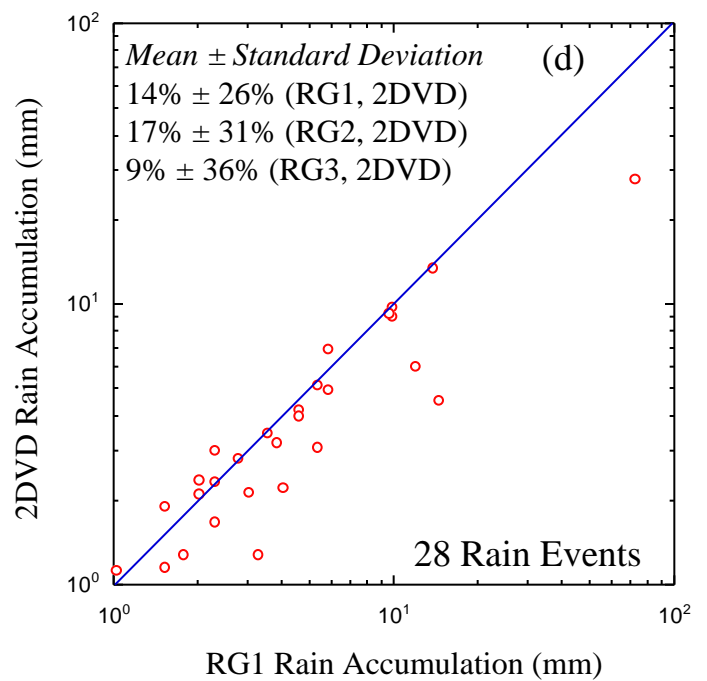
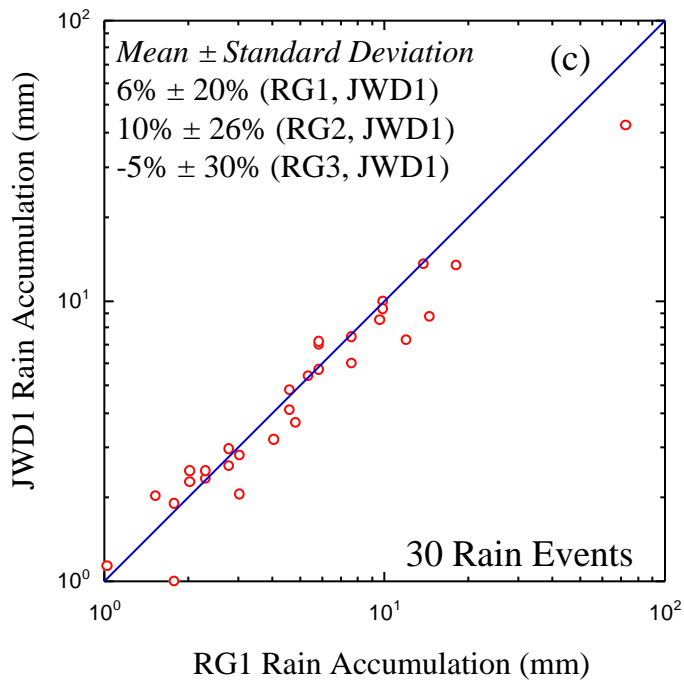
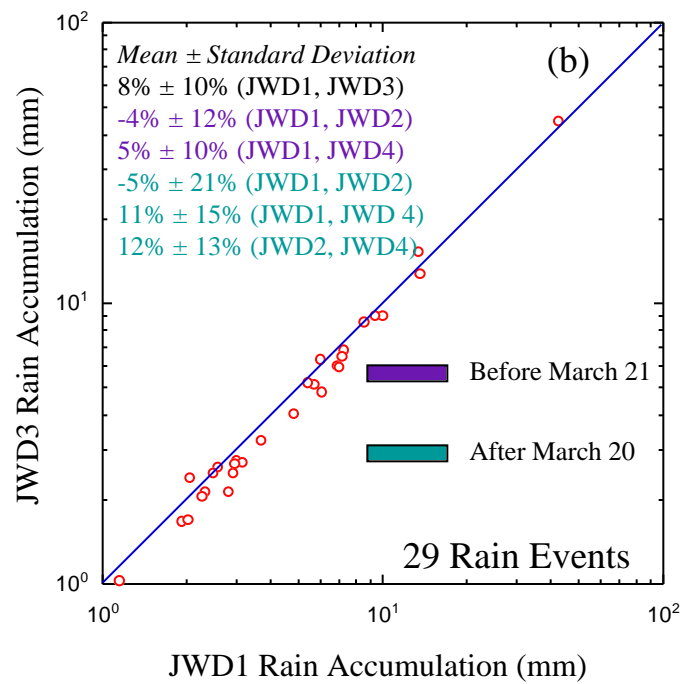
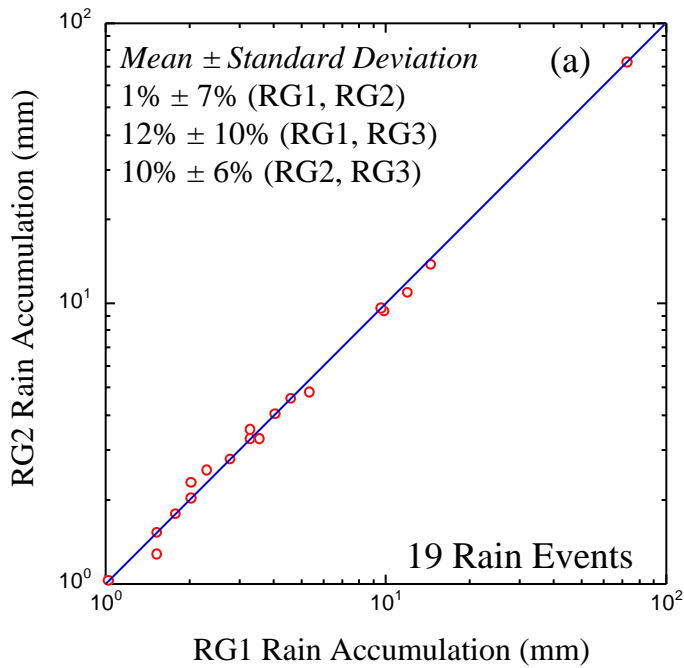


Figure 6. One-to-one comparison of rain accumulation of the rain gauges (a), of the impact disdrometers (b), rain gauges and impact disdrometers (c), and rain gauges and the optical disdrometer (d). The rain accumulation statistics (mean and standard deviations) are also given for each pair of comparisons.

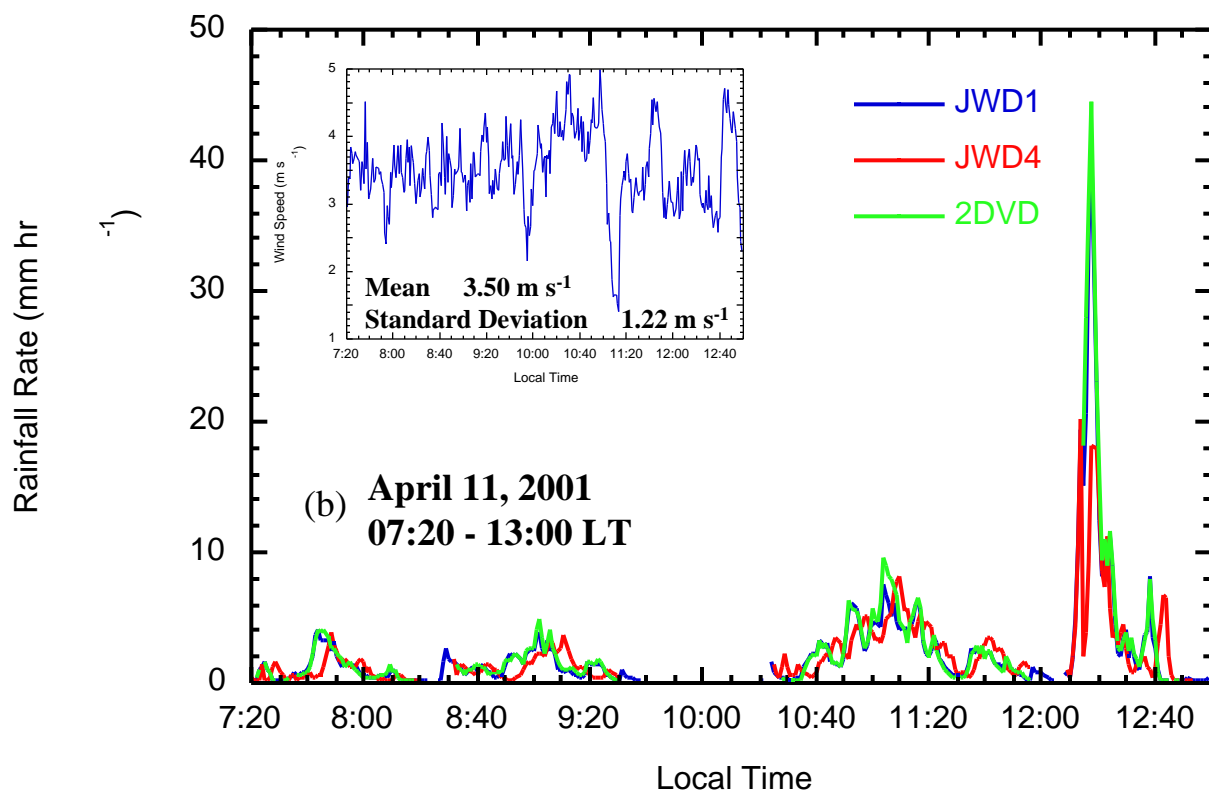
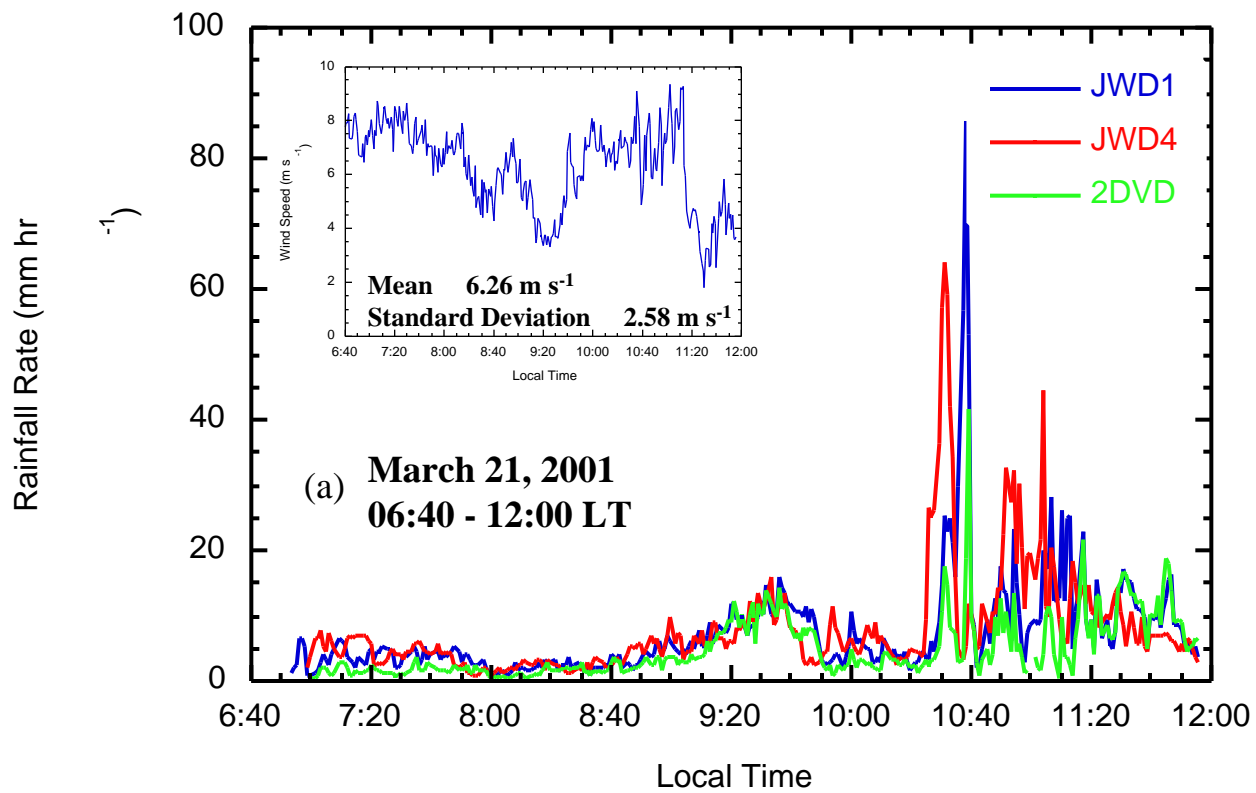


Figure 7. Rainfall time series of JWD1, JWD2, and 2DVD for (a) March 21 and (b) April 11 rain events. The corresponding time series of wind speed are also given.

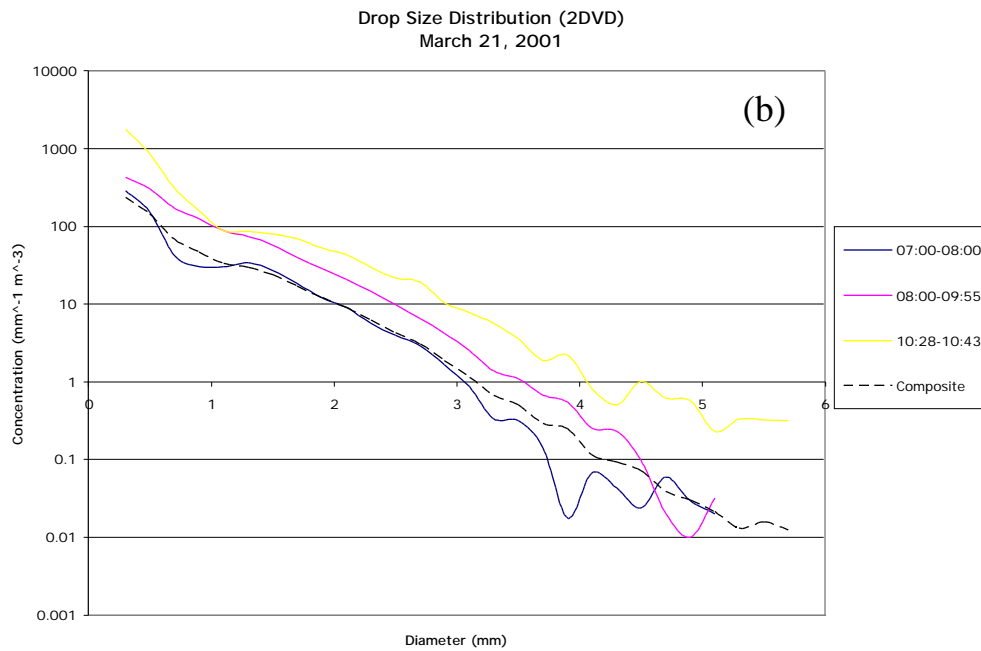
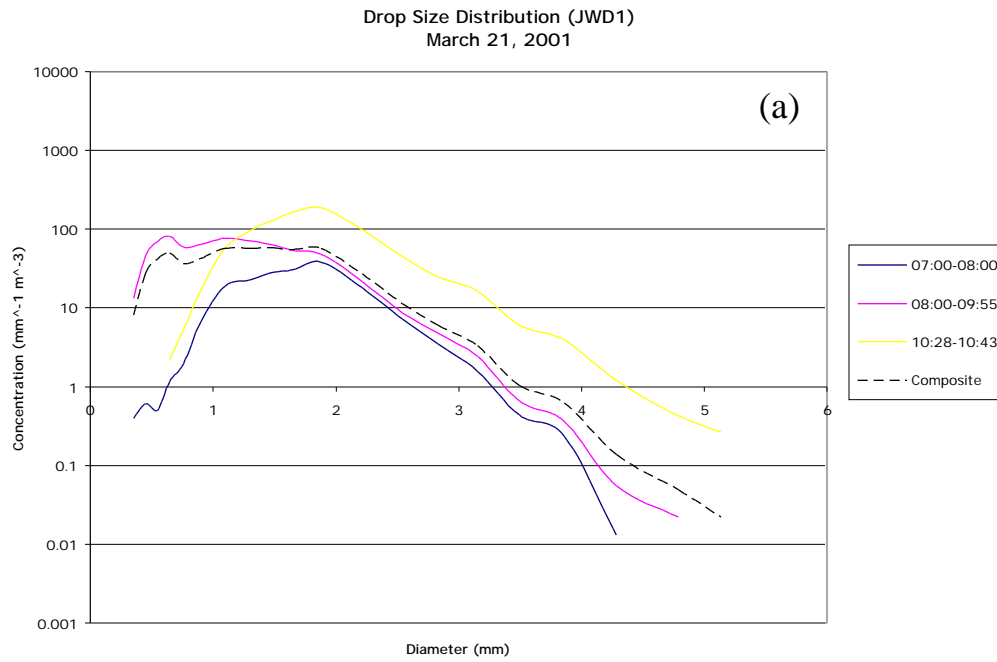


Figure 8. The drop size distributions for the selected time periods of March 21 rain event. The distributions are shown for both JWD1 (a) and 2DVD (b) measurements.

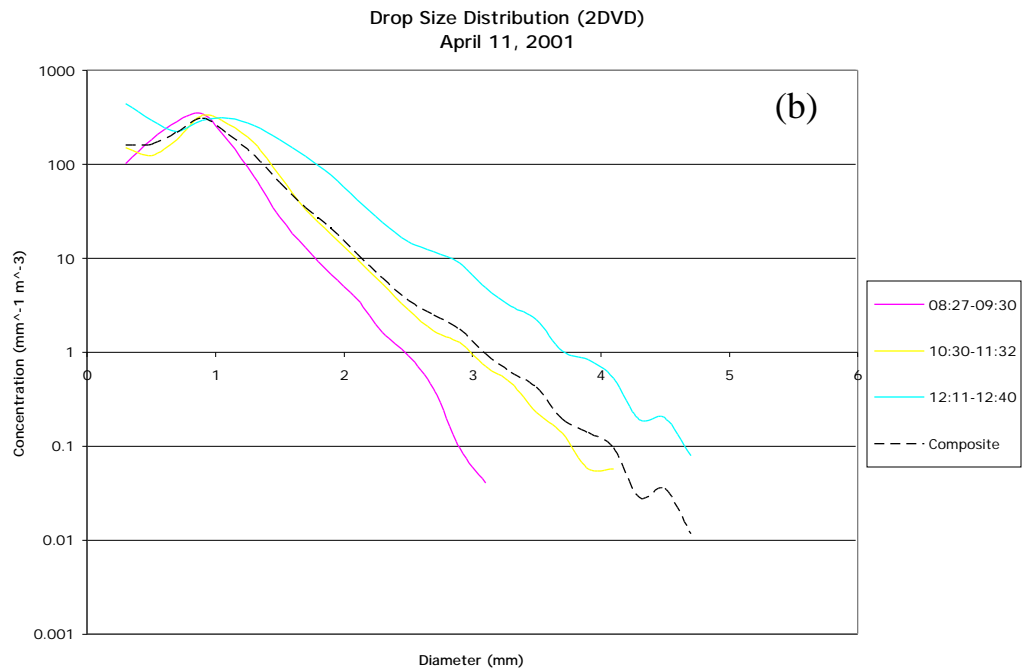
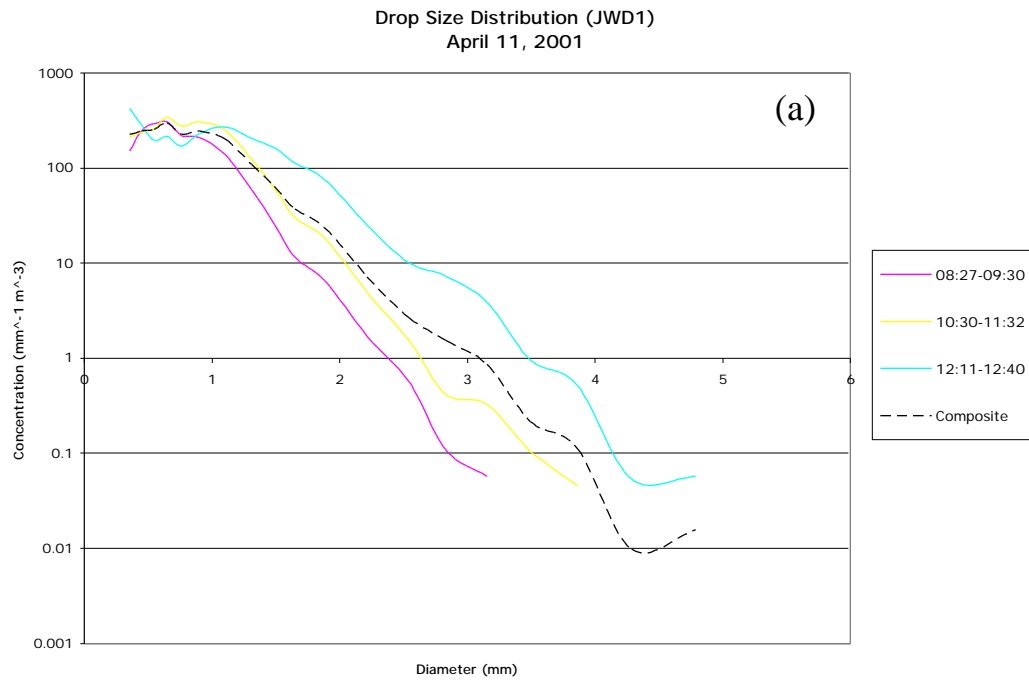


Figure 9. The drop size distributions for the selected time periods of April 11 rain event. The distributions are shown for both JWD1 (a) and 2DVD (b) measurements.

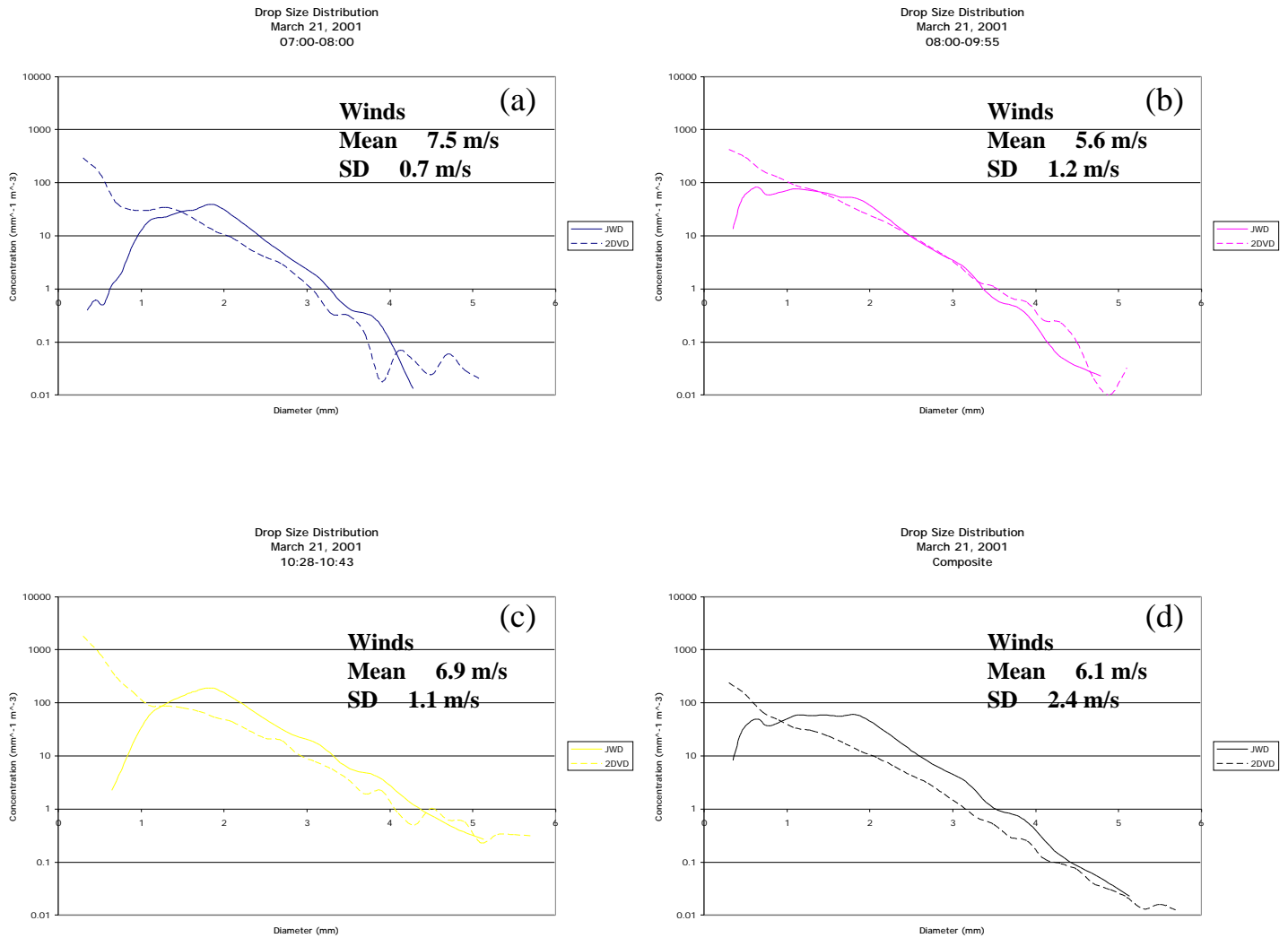


Figure 10. The JWD versus 2DVD drop size distributions for the selected time periods of March 21 rain event. The corresponding wind speed statistics are also given.

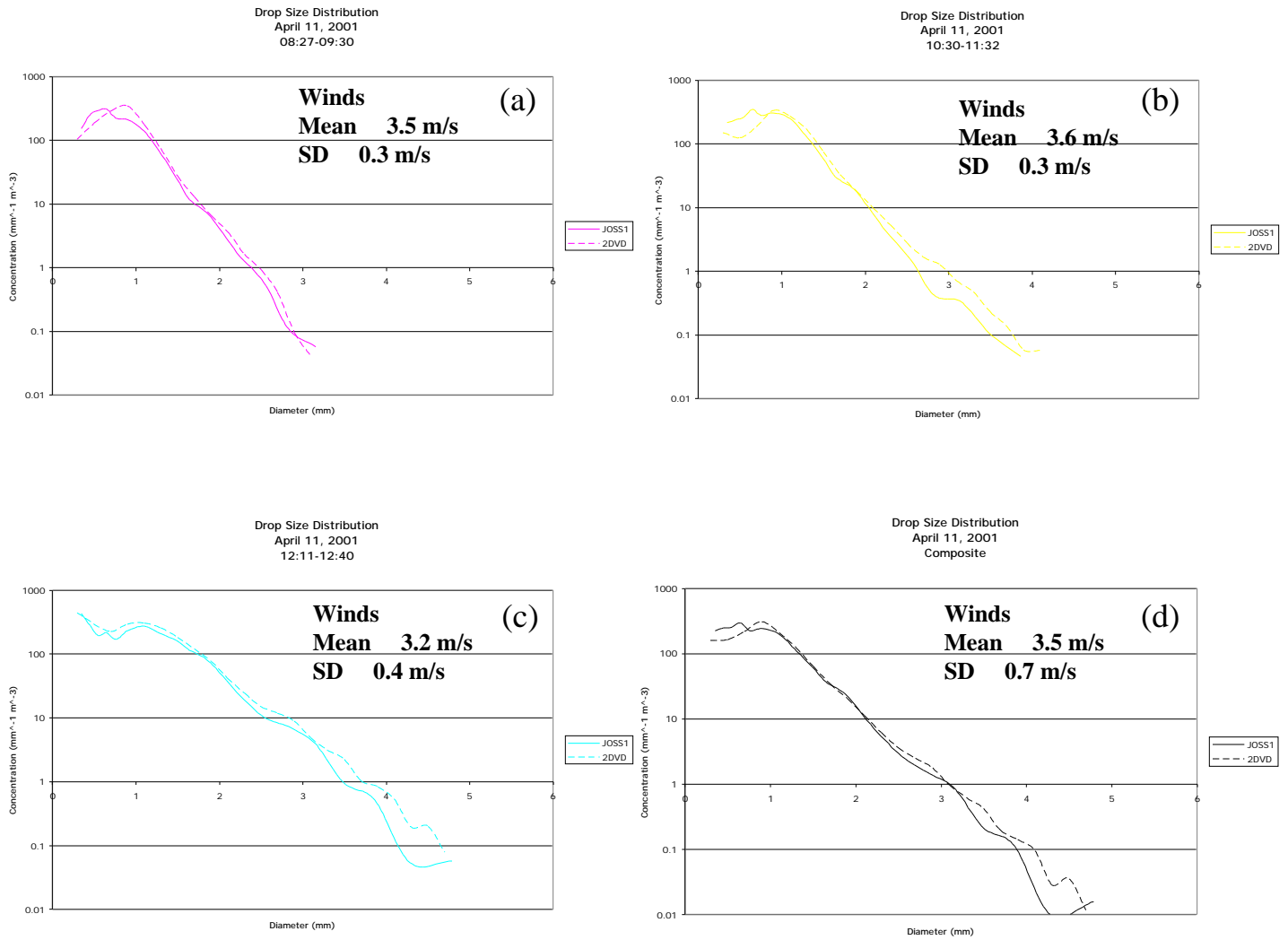


Figure 11. The JWD versus 2DVD drop size distributions for the selected time periods of April 11 rain event. The corresponding wind speed statistics are also given.

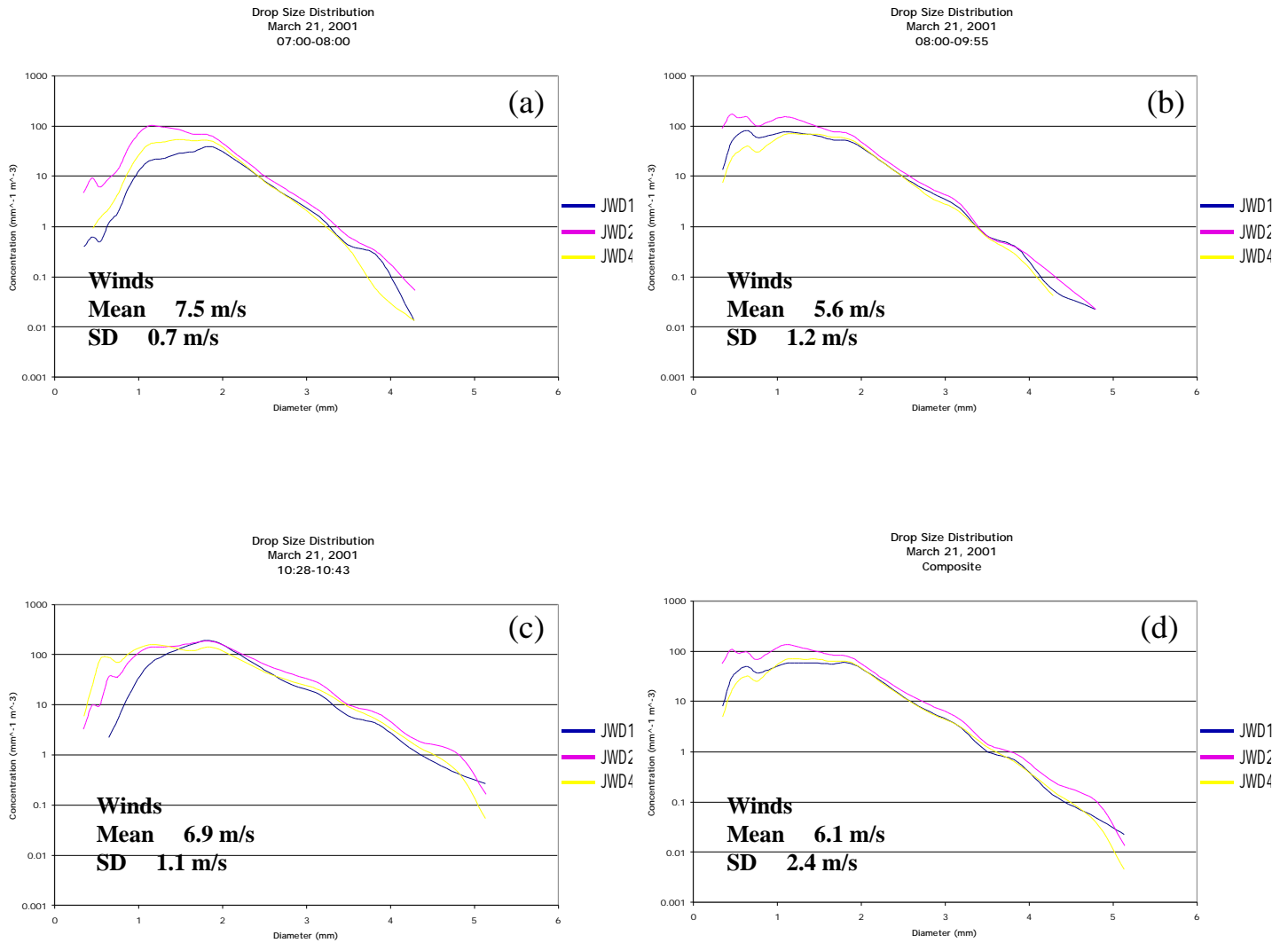
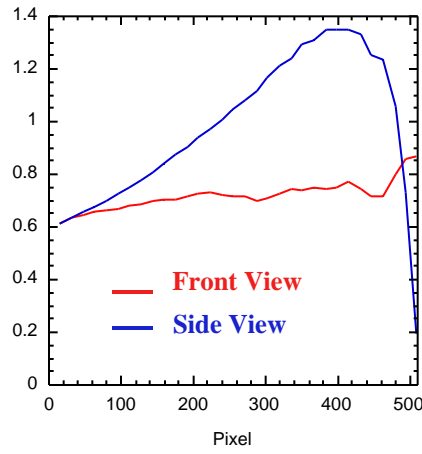
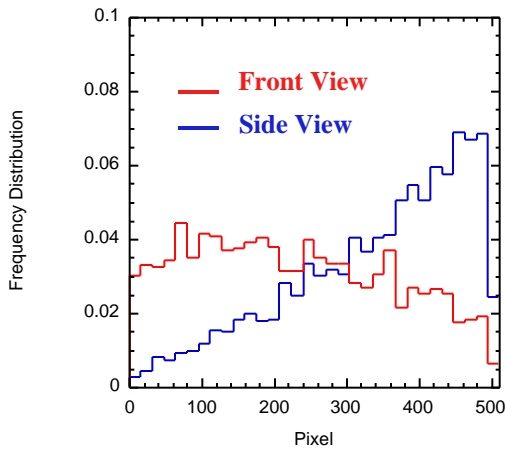
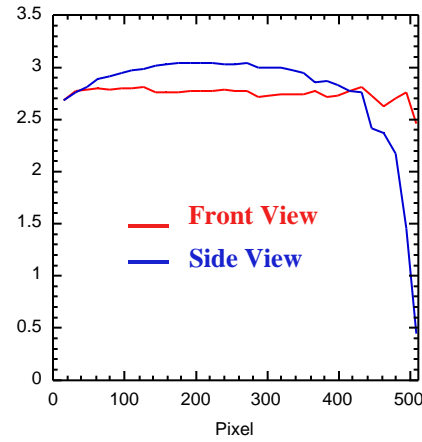
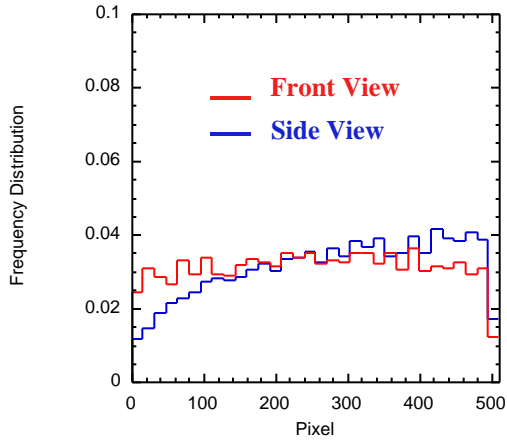


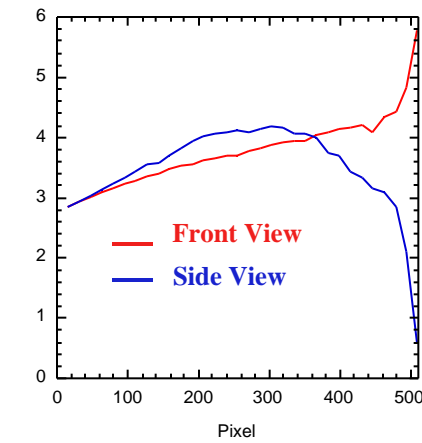
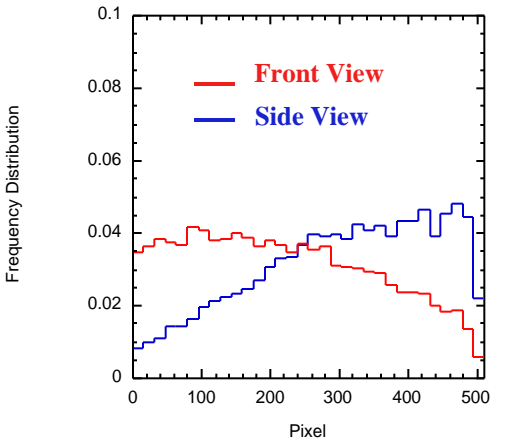
Figure 12. The drop size distributions for the selected time periods of the March 21 rain event. Each graph corresponds to three different disdrometer measurements separated at certain distances.



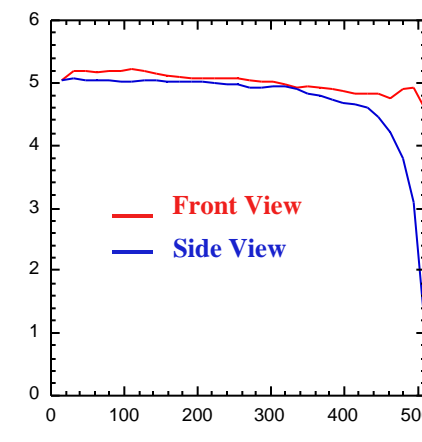
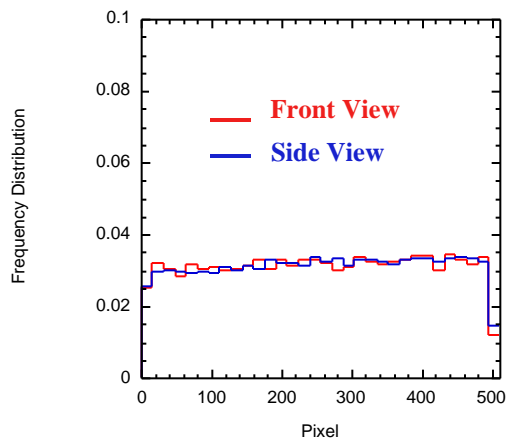
(a)
07:07 - 07:30 LT
March 21, 2001



(b)
09:12 - 09:32 LT
March 21, 2001



(c)
10:24 - 10:42 LT
March 21, 2001



(d)
12:11 - 12:40 LT
April 11, 2001

Figure 13. The distributions of the drops for front and side view of the 2DVD plane. The rain accumulations calculated at different sample areas are also shown.

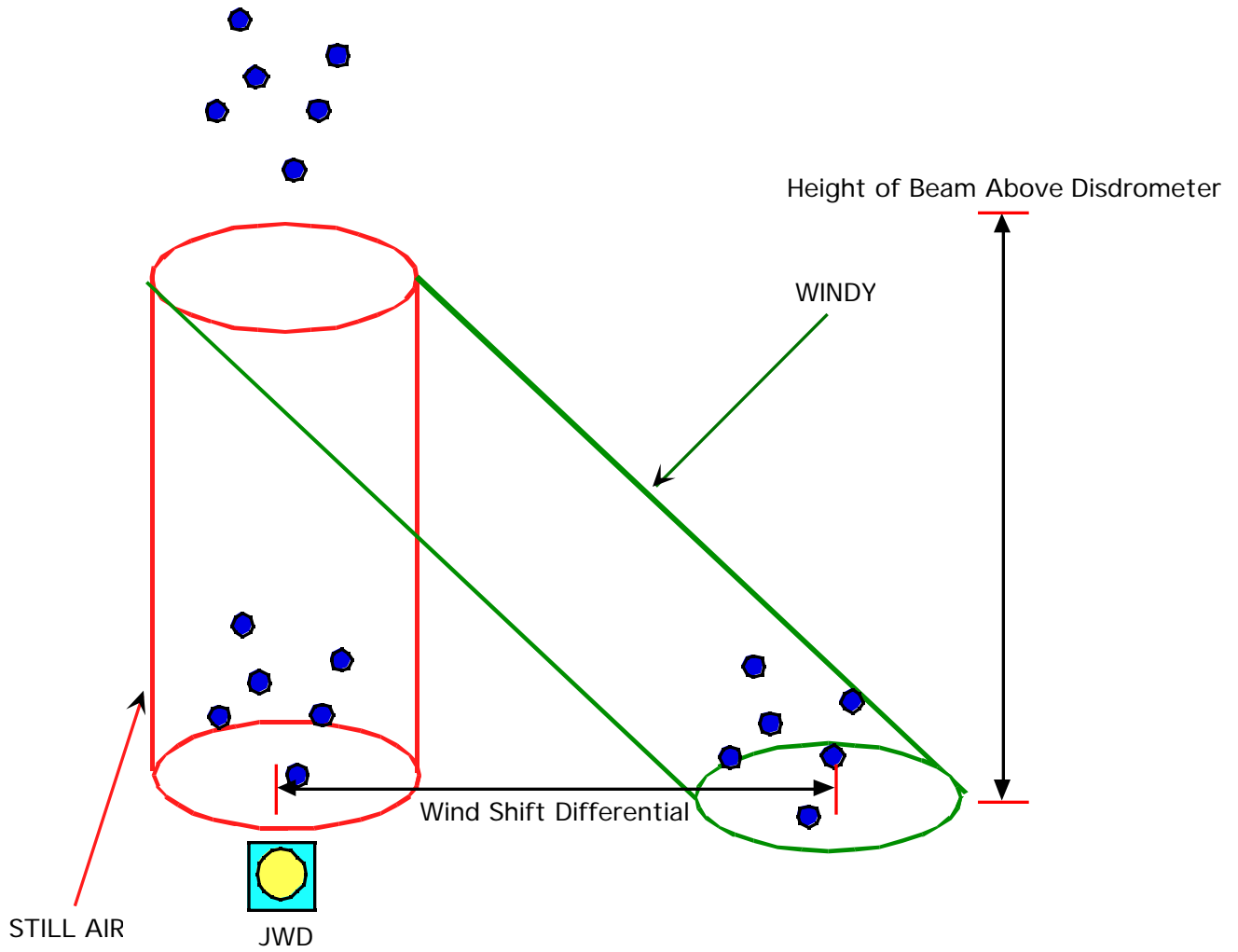


Figure 14. A schematic diagram of the differential wind shift effect on radar and disdrometer rainfall comparison.

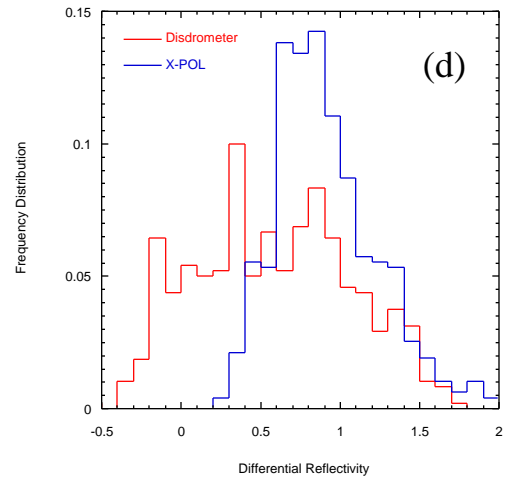
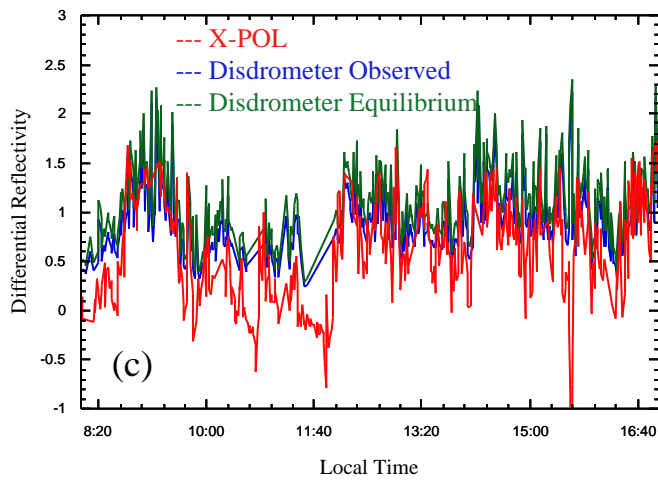
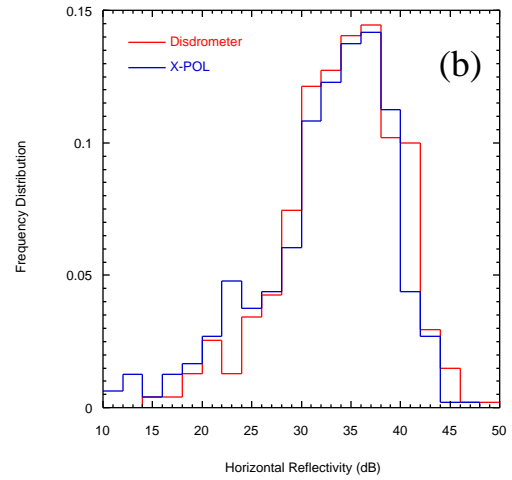
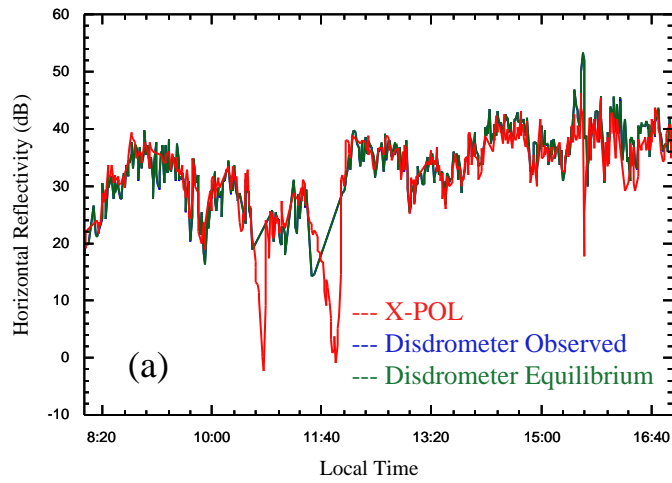


Figure 15. Time series of horizontal reflectivity (a) and of differential reflectivity (c) through X-POL radar and JWD1 measurements. The distributions of the horizontal reflectivity (b) and differential reflectivity (d) for both X-POL and JWD1 measurements are also given.